Magnetism in AV_3Sb_5 (A = Cs, Rb, K): Complex landscape of dynamical magnetic textures

Debjani Karmakar,[1,2,*,†] Manuel Pereiro,[1,*] Md. Nur Hasan,[3] Ritadip Bharati,[4] Johan Hellsvik,[5] Anna Delin,[6,7] Samir Kumar Pal,[3] Anders Bergman,[1] Shivalika Sharma,[8] Igor Di Marco,[1,8,9] Patrik Thunström,[1] Peter M. Oppeneer,[1] and Olle Eriksson[1,‡]

[1]*Department of Physics and Astronomy, Uppsala University, Box 516, SE-751 20 Uppsala, Sweden*
[2]*Technical Physics Division, Bhabha Atomic Research Centre, Mumbai 400085, India*
[3]*Department of Chemical and Biological Sciences, S. N. Bose National Centre for Basic Sciences, Block JD, Sector-III, SaltLake, Kolkata 700 106, India*
[4]*School of Physical Sciences, National Institute of Science Education and Research, Homi Bhabha National Institute (HBNI), Jatni, 752050 Odisha, India*
[5]*PDC Center for High Performance Computing, KTH Royal Institute of Technology, SE-100 44 Stockholm, Sweden*
[6]*Department of Applied Physics, KTH Royal Institute of Technology, SE-106 91 Stockholm, Sweden*
[7]*Swedish e-Science Research Center (SeRC), KTH Royal Institute of Technology, SE-10044 Stockholm, Sweden*
[8]*Asia Pacific Center for Theoretical Physics, Pohang 37673, Republic of Korea*
[9]*Department of Physics, Pohang University of Science and Technology, Pohang 37673, Republic of Korea*

(Received 18 July 2023; accepted 11 October 2023; published 9 November 2023)

We have investigated the dynamical magnetic properties of the V-based kagome stibnite compounds by combining the *ab initio*-extracted magnetic parameters of a spin-Hamiltonian, like inter-site exchange parameters, magnetocrystalline anisotropy and site projected magnetic moments, with full-fledged simulations of atomistic spin- dynamics. Our calculations reveal that, in addition to a ferromagnetic order along the [001] direction, the system hosts a complex landscape of magnetic configurations comprised of commensurate and incommensurate spin spirals along the [010] direction. The presence of such chiral magnetic textures may be the key toward solving the mystery about the origin of the experimentally observed inherent breaking of the C_6 rotational, mirror, and the time-reversal symmetry.

DOI: 10.1103/PhysRevB.108.174413

For the V-based kagome stibnites, AV_3Sb_5 (A = Cs, Rb, K), a complete picture of the origin of the experimentally observed spontaneously broken time-reversal as well as C_6 rotational symmetries and their respective interplay with the underlying magnetic structure is missing. This lacuna has proliferated into wide variations of inconclusive explanations toward the experimental results like muon spin-rotation (μSR) or the anomalous Hall effect (AHE) [1,2]. In the zero-field μSR spectra, the depolarization function of single crystals of these materials deviate from the standard Gaussian Kubo-Toyabe behavior, for which the possible reasons may be (a) an inhomogeneous distribution of the nuclear moments, (b) the presence of an electric field gradient due to a chiral charge order (CO), or (c) a contribution of purely electronic origin emanating from the chiral distribution of the spin moments [1]. Below the CO transition and at high field, the significant increase of the rate of spin relaxation of muons and the enhanced spread of the internal fields are suggested to be the experimental signatures of a broken time-reversal symmetry enrooted to their electronic attributes [1]. In the same vein, the experimentally observed giant AHE for this series exhibits an anomalous Hall ratio, which is an order of magnitude higher than that of intrinsic magnetic systems like body-centered cubic Fe [3]. The nature of the AHE is proposed to be of extrinsic type related to the spin fluctuations across the triangular V clusters leading to an enhanced skew scattering [2]. Currently proposed microscopic mechanisms behind the nature of the μSR spectra, the giant AHE, and their interconnection with the broken C_6 rotational- and time-reversal symmetries are far from conclusive, suggesting a wide variety of reasons, viz., the presence of orbital current, electron nematicity, or a 2×2 charge modulation producing chiral charge density waves [1–3]. The effects of spin-density wave, complex spin texture, and dynamical magnetic ground states on the CO and the broken symmetries therein are yet to get analyzed.

In the recent literature, there are controversies regarding the presence of broken time-reversal symmetry in the first member of this kagome superconducting series, viz., CsV_3Sb_5. Saykin *et al.* [4] have used high-resolution polar Kerr effect measurements to demonstrate an absence of any observable Kerr effect in CsV_3Sb_5, which poses a question

*These authors contributed equally to this work.
†Corresponding author: debjani.karmakar@physics.uu.se
‡Corresponding author: olle.eriksson@physics.uu.se

mark against the presence of spontaneous breaking of time-reversal symmetry in this compound. On the other hand, albeit being centrosymmetric, this system reveals chiral transport behavior via second harmonic generation under an in-plane applied magnetic field [5], implying an inherently broken mirror symmetry. Such an occurrence of electronic magnetochiral anisotropy is prominent <35 K and thereby indicates interplay of time-reversal symmetry breaking and electronic chirality in CsV_3Sb_5 below this transition temperature.

The two-dimensional (2D) kagome lattice with nearest-neighbor (NN) antiferromagnetic (AFM) exchange interactions (J) is a well-known archetype of inherently frustrated systems, where it is impossible to optimize all exchange interactions. Here, after including diverse NN interactions, a panoply of degenerate magnetic ground states may arise, where the out-of-plane AFM or ferrimagnetic order competes with the coplanar 120° structures with uniform or staggered chirality [6,7]. Depending on the temperature (T), their magnetic ground states encompass three different regimes, viz., (i) a spin-diffusive paramagnetic regime ($T > |J|$), (ii) an intermediate cooperative regime leading to a spin-liquid arrangement ($0.001|J| < T < |J|$), and (iii) an ultralow temperature coplanar regime ($T < 0.001|J|$). The first crossover at $T \sim J$ may have a finite local spin correlation without any long-range order (LRO), and for the second one at $T \sim 10^{-3}J$, the entropic selection favors a coplanar order with anisotropic dynamics [8–11]. For the coplanar configuration, thermal or quantum fluctuations resolve the ground-state degeneracy after stabilizing a LRO in the *order-by-disorder* process [11], the most common of which is the 120° spin texture. With increasing temperature, such chiral LRO is intervened after generation of weathervane defects, leading to the rotational staggering of spins around the local spin axis [6].

The series AV_3Sb_5, as suggested from their complex magnetic spectral functions [12], is an itinerant-electron system with a correlated electronic structure. The low-energy magnetic excitations of such systems can be evaluated via a multiscale approach upon satisfaction of three conditions, viz., (1) the magnetic configurational energy dependence can be mapped onto a generalized Heisenberg model Hamiltonian $H = -\sum_{i \neq j} e_i^{\alpha} \hat{J}_{ij}^{\alpha\beta} e_j^{\beta}$, $\alpha, \beta = x, y, z$, with the unit vector $\mathbf{e}_i$ designating the local spin direction at the ith site, (2) the exchange tensor $\hat{J}_{ij}^{\alpha\beta}$ can be calculated from first principles, and (3) the ground-state many-electron systems rely on the adiabatic approximations, with decoupled faster process of intersite electronic hopping from the slower moving magnetic excitations or frozen magnons [13]. In our prior study on this system [12], the fully relativistic exchange tensor was reported using the Lichtenstein-Katnelson-Antropov-Gubanov (LKAG) formalism coupled to the dynamical mean field theory (DMFT) [14–20]. The tensor possesses terms like the symmetric-isotropic Heisenberg (J_{ij}), antisymmetric and anisotropic Dzyaloshinskii-Moriya (DM), and symmetric-anisotropic Heisenberg interactions (Γ). The DM and Γ interactions are calculated by using relations like $D_{ij}^{z} = \frac{1}{2}(\hat{J}_{ij}^{xy} - \hat{J}_{ij}^{yx})$, $\Gamma_{ij}^{z} = \frac{1}{2}(\hat{J}_{ij}^{xy} + \hat{J}_{ij}^{yx})$ and analogous ones for the x and y components. Figure 1 presents the plots of the intersite exchange interactions for various shells of NN V-based stibnites extracted with an FM interlayer interaction. The negative values of J_{ij} correspond to an AFM coupling. A closer scrutiny of this figure reveals that the magnetic interactions in this system are composed of various competing mechanisms. For the first NN shell, the J_{ij} values are roughly two orders of magnitude larger than the D_{ij} and Γ_{ij} values. However, from the next-NN shell, the anisotropic interactions D_{ij} and Γ_{ij} become comparable with J_{ij}. Such a competing environment of complex magnetic interactions can be a fertile ground for obtaining chiral magnetic ground states. It may also be mentioned in passing that, for metallic and Mott insulating kagome systems, chiral magnetism may indeed appear from a very simple correlated Hamiltonian [21,22]. Moreover, at the same NN distances, the flipping sign of D_{ij} implies a signature of the chiral magnetic textures as per the Moriya rule.

To obtain inversion asymmetric chiral environments with significant D_{ij} and Γ_{ij}, systems were artificially designed using metallic multilayers like Mn/Cr/W[110] or Pd-Fe/Ir[111] involving components of high spin-orbit coupling (SOC) [23–26]. Recently, such spiral magnetic textures have gained attention by virtue of their additional capability to explore the topological spin transport via skyrmions [25,26] for spin-torque devices [27–29]. Here, the limitations introduced by the instabilities like Walker breakdown on the mobility of the domain walls can be escaped by reaching the supermagnonic regime [28–32]. A sustained search for such chiral magnetic systems constitutes an active area of research. In this paper, we demonstrate that the V-based stibnite kagome system, with the presence of local moments and a balanced competition between the intersite exchanges and SOC, constitutes a breeding ground for long-period, inhomogeneous chiral magnetic superstructures.

The ground-state magnetic properties of complex magnetic systems are derived after constructing a classical atomistic spin model, where the bilinear effective Hamiltonian can be written as $\mathcal{H}_{\text{mod}}^{i,j} = -J_{ij}\mathbf{e}_i \cdot \mathbf{e}_j - \mathbf{D}_{ij}\mathbf{e}_i \times \mathbf{e}_j - \mathbf{e}_i\Gamma_{ij}\mathbf{e}_j - \kappa \sum_{k=i,j} (\mathbf{e}_k \cdot \mathbf{e}_k^r)^2$ [27,33,34]. Here, $\mathbf{e}_i$ and $\mathbf{e}_j$ are normalized atomic spin moments at the atomic sites i and j, and $\mathbf{e}_k^r$ is the easy axis along the arbitrary unit vector $\mathbf{r}$. The four different terms of this Hamiltonian represent the energies corresponding to the isotropic Heisenberg interaction (J), the DM interaction (DM), the symmetric-anisotropic exchange interaction (Γ), and the magnetocrystalline anisotropy (K) [24].

In a periodic lattice, the most general solution of this model generates a homogeneous spin spiral, where the angle between the resultant spin moments of two adjacent neighbors are constant throughout the spiral [35]. The atomic-site (i) spin moments of such a spin spiral can be mapped onto a unit circle with $1 \leqslant i \leqslant N$, with N being the number of atomic spins in a spiral, the pitch of which can be defined as $\lambda = Na$, with a being the lattice constant. The chirality of the spiral is dependent on the clockwise (negative) or anticlockwise (positive) directionality of the mapping. Naturally, the DM interaction has a significant role in determining the chirality of the spiral [23–26].

The simultaneous presence of SOC and large number of magnetic atoms render the first-principles treatment of a long-pitched spin spiral computationally taxing [7,29]. Therefore, for chiral magnetic systems [24,36], a continuum

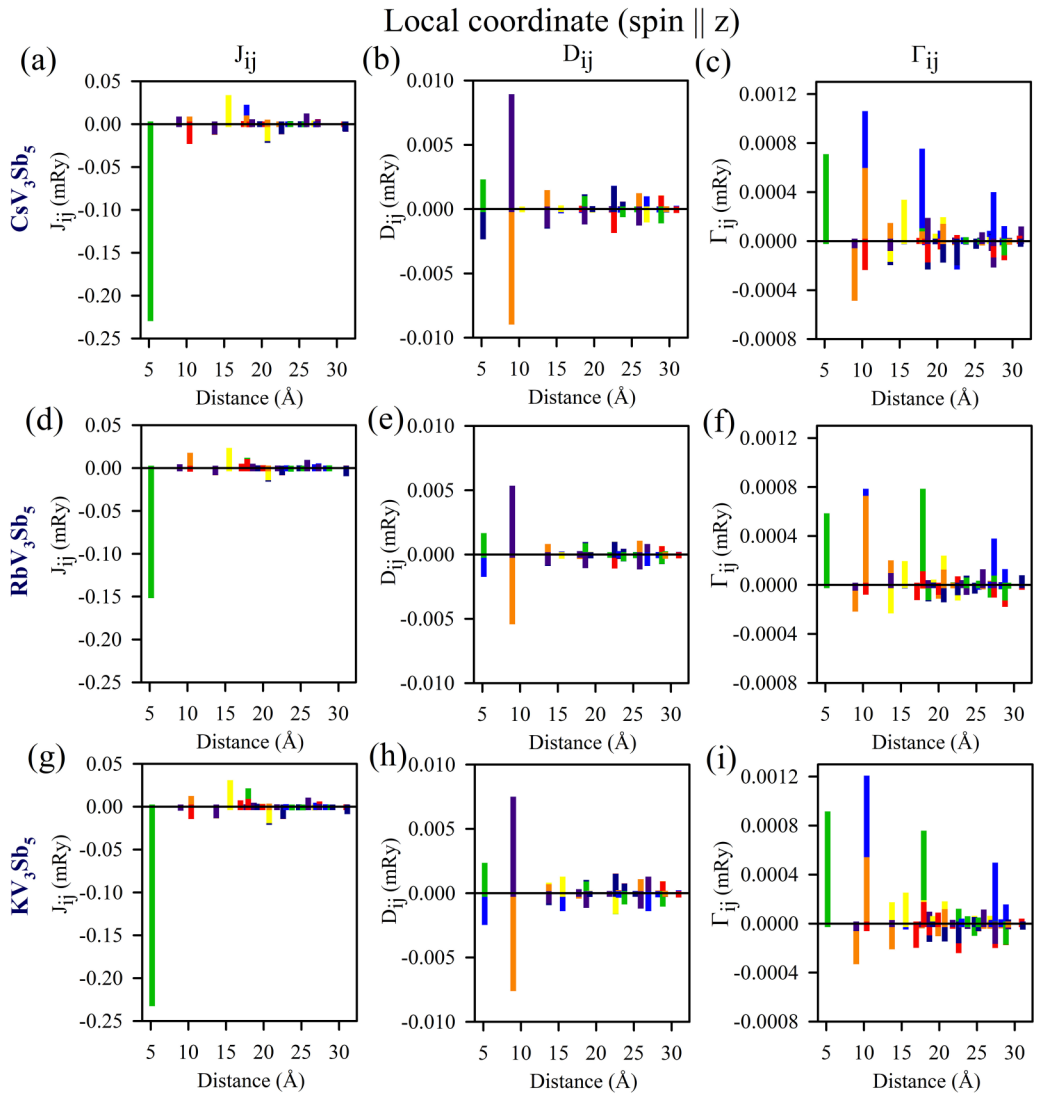

FIG. 1. The intersite exchange parameters as a function of nearest-neighbor (NN) distances in local coordinate system: J_{ij}, D_{ij}, and Γ_{ij} for (a)–(c) CsV_3Sb_5, (d)–(f) RbV_3Sb_5, and (g)–(k) KV_3Sb_5. Note that, for some NN distances, we have different strengths of the interactions in different directions, implying anisotropy in the directional distribution of the interactions. The difference in color at the bar plot signifies the difference of the strength of various magnetic exchange interactions at a particular value of NN distance.

micromagnetic model is defined, where the energy of the spin spiral is written in terms of the local magnetization vector $\mathbf{m}$ as $E[m] = \frac{1}{\lambda}\int_0^{\lambda} dx[\frac{A}{4\pi^2}(\dot{\mathbf{m}})^2 + \frac{\mathbf{D}}{2\pi}\cdot(\mathbf{m}\times\dot{\mathbf{m}}) + \mathbf{m}^T\kappa\mathbf{m}]$. Here, A, $\mathbf{D}$, and κ are the spin-stiffness constant, the effective DM vector, and the anisotropy tensor, respectively, while $\dot{\mathbf{m}}$ is the gradient of the magnetization. For a generalized spin spiral with a wave vector $\mathbf{q}$, this magnetic moment $\mathbf{m}$ at a given atomic position $\mathbf{R}_{n\alpha}$ can be written in the tensor format as $\mathbf{m}_{n\alpha} = m_\alpha \begin{bmatrix} \sin\theta_\alpha\cos(\varphi_{n\alpha}+\gamma_\alpha) \\ \sin\theta_\alpha\sin(\varphi_{n\alpha}+\gamma_\alpha) \\ \cos\theta_\alpha \end{bmatrix}$ [5,24]. Here, θ_α and γ_α are the cone and phase angles, respectively. The azimuthal angle corresponding to the local magnetic moment can be calculated as $\varphi_{n\alpha} = \mathbf{q}\cdot\mathbf{R}_{n\alpha}$. Such spiral magnetic ground states can be either commensurate or incommensurate with the underlying lattice, the solution of which can be obtained by following Petit's method [37], using a series of effective coordinate transformations of the local spins into a ferromagnetic (FM) order [37,38].

For the present kagome series, the atomistic descriptions of the spin moments can be used to construct the spin model because of its sufficiently localized electronic densities around the atomic sites and the invariance of the resultant atomic spin moments with respect to their orientations. The chiral ground states can be obtained by dynamically solving the atomistic model where, at every magnetic site, around the direction of the classical spin, the dynamics of the small fluctuations of the spins are calculated following the implementations in the UppASD software [34].

The spin-spin correlation functions and their Fourier transform, alias the dynamical structure factor, also accessible experimentally by inelastic neutron scattering, can be calculated as $S(q,\omega) = \frac{1}{2\pi N}\sum_{i,j}\exp[\iota q(r_i - r_j)]\int_{-\infty}^{\infty} d\tau\exp(-\iota\omega\tau)\langle \mathbf{e}_i\mathbf{e}_j(\tau)\rangle$, where

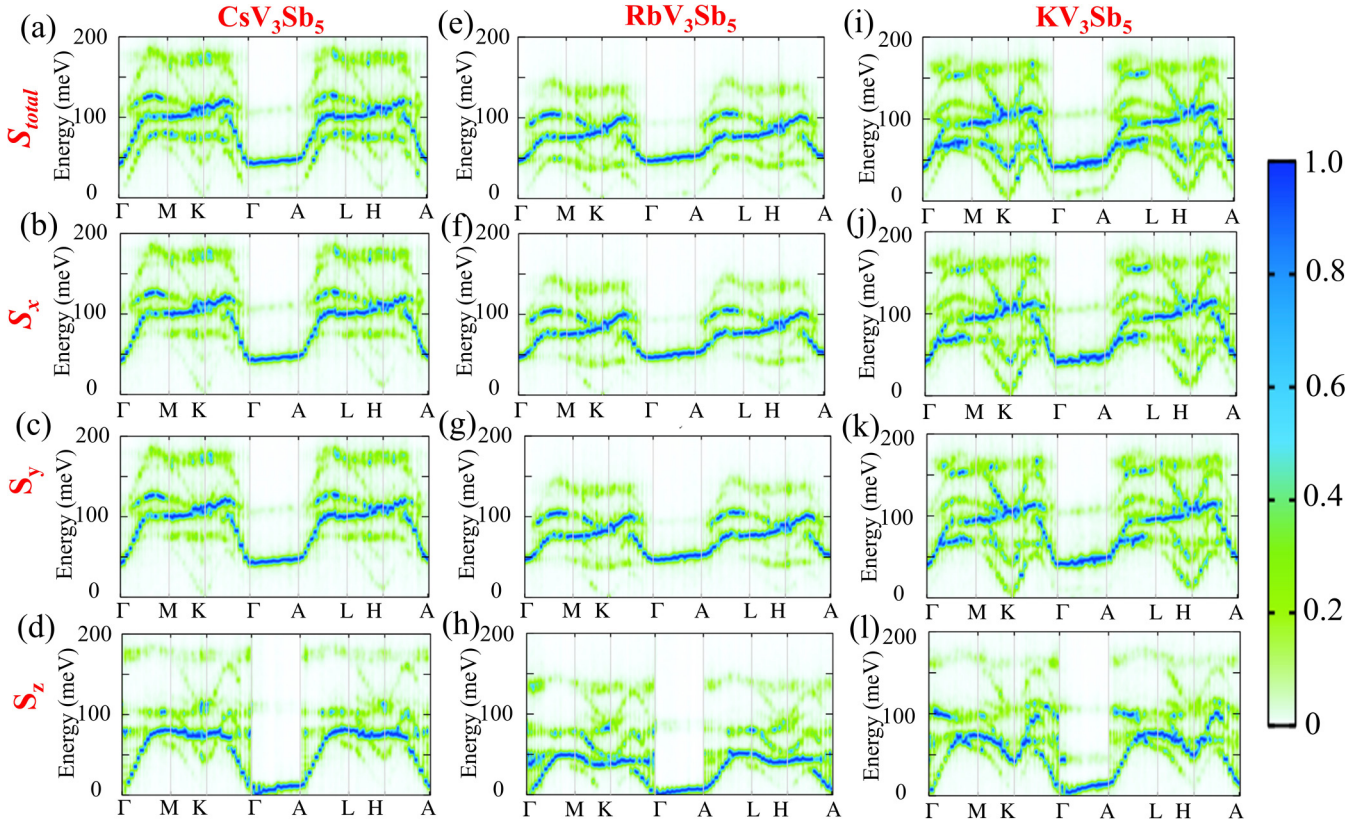

FIG. 2. The dynamical structure factors $S(q, \omega)$ plotted along the high-symmetry paths: (a), (e), and (i) the resultant total; (b), (f), and (j) S_x projected; (c), (g), and (l) S_y projected; and (d), (h), and (l) S_z projected $S(q, \omega)$ for CsV_3Sb_5, RbV_3Sb_5, and KV_3Sb_5, respectively. The dynamical spin correlations shown in the figure are those around the magnetic excitation energy minimum at the K point.

$\mathbf{r}_i$ is the position vector of the magnetic atoms, and $\mathbf{e}_i$ is the local spin vector. For the incommensurate spin structures, in addition to $\omega(q)$, the magnon dispersion also constitutes modes like $\omega(q \pm Q)$, and the corresponding correlations $S(q, \omega)$ and $S(q \pm Q, \omega)$ describe rigid rotations on the ordering plane and the canting with respect to the same plane, respectively [38], where Q is the ordering wave vector.

Figures 2(a)–2(i) represent the spin-component projected dynamical structure factors $S(q, \omega)$ calculated for the q values along the high-symmetry paths for CsV_3Sb_5 (CVS), RbV_3Sb_5 (RVS), and KV_3Sb_5 (KVS), respectively, after considering the full Hamiltonian. The highest values of the spin correlations are obtained along the adiabatic magnon dispersion lines, which in Fig. 2 are represented by the transition in color from green to blue in the adjacent color scale. The kagome system in its unit cell possesses 3 V atoms, and in the full noncollinear manner, the three possible magnetic orientations should give rise to nine modes. However, along the Γ-A direction, the out-of-plane magnon dispersions are triply degenerate. In addition, the x and y components of the structure factor show the minimum of the energy dispersion at the K point rather than the Γ point, indicating that their magnetic ground state collapses into a spin-spiral state. This state is shown in Figs. 3(a)–3(c) and is analyzed in more detail below. The x and y components of $S(q, \omega)$ have significant values of the magnon gap at the Γ point. The z component and thus the total dynamical structure factor display a much smaller value of the gap. The reason behind this gap is the high value of the magnetocrystalline anisotropy, amounting to 0.29, 0.22, and 0.28 mRy per V atom for CVS, RVS, and KVS, respectively, as per the DFT + DMFT + SOC calculations. The derived anisotropy parameters indicate that all three systems display a uniaxial, out-of-plane easy-axis pattern of spin orientations.

The spin textures of the dynamically obtained magnetic ground states after solving the full Hamiltonian with all J, DM, Γ, and K terms are plotted in Figs. 3(a)–3(c). The corresponding spin arrangements in the star-of-David kagome pattern are plotted in Figs. 3(d)–3(f) with the magnetization densities in Figs. 3(g)–3(i). The color scale of Fig. 3 represents the values of the normalized out-of-plane (z) projections of the spins. This figure evidences that the dynamical magnetic ground states of CVS and RVS are similar, manifesting a superposition of three types of underlying magnetic orders, viz., a FM arrangement along the [001] direction and two spin-spiral configurations, viz., one commensurate and the other incommensurate spin-spiral arrangements along [010]. The pitches corresponding to the commensurate and incommensurate spin spirals are calculated to be $3a$ and $1.5a$, respectively, with a being the lattice parameter. The ground-state spin texture of KVS, as seen in Fig. 3(c), consists of additional complexities, viz., a superposition of (i) FM order along [001], (ii) one commensurate spin spiral along [010], and (iii) two more interpenetrating commensurate spirals along [010]. The pitches of all these spirals are $3a$. In Figs. S1 and S2 in the Supplemental Material (SM) [39], the calculations

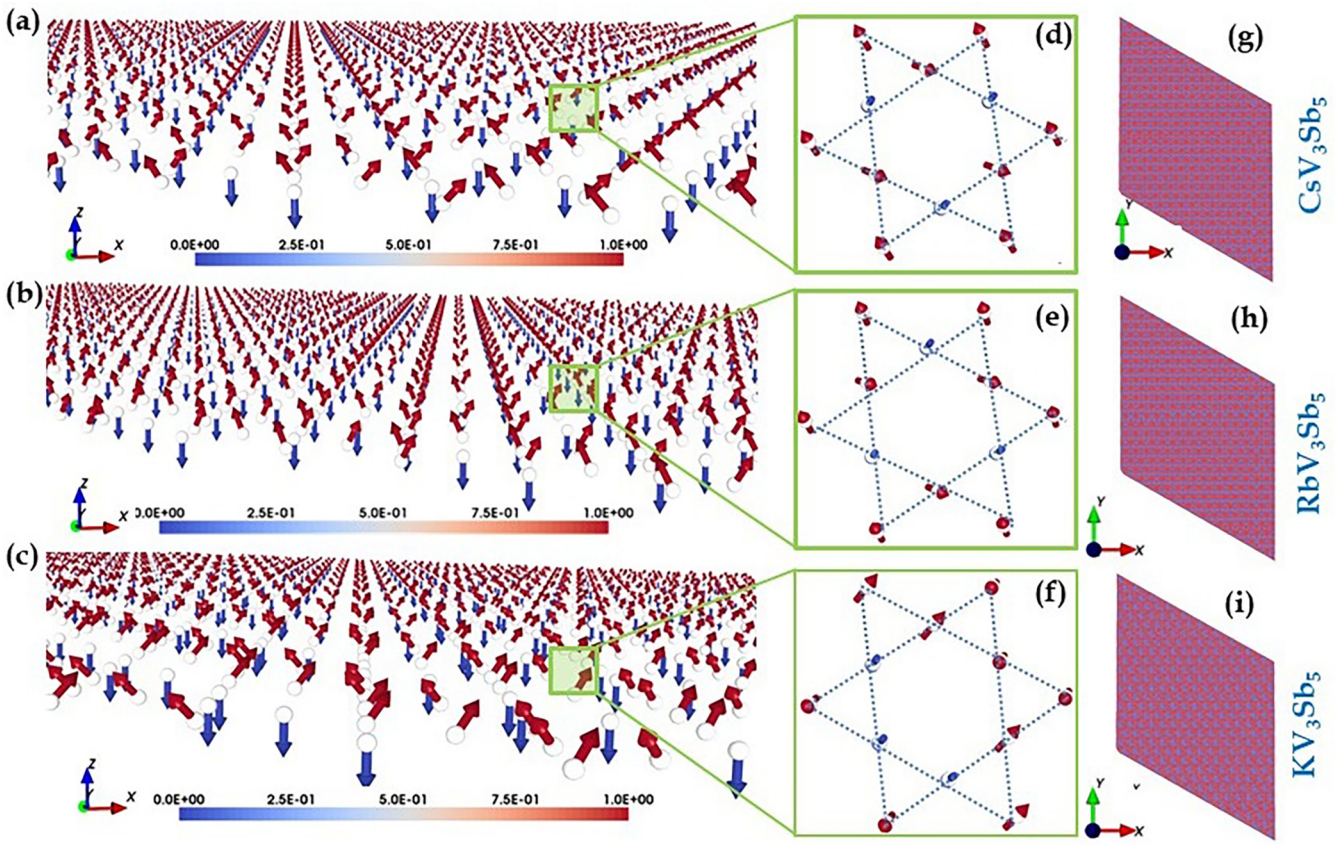

FIG. 3. (a)–(c) The three-dimensional (3D) view of the dynamical ground-state spin textures obtained from the $J + K + \Gamma +$ DM Hamiltonian, (d)–(f) spin configurations on the star of David of the kagome lattice, and (g)–(i) the corresponding magnetization densities for CVS, RVS, and KVS, respectively. The color bars associated with the spin textures indicate the projection of the magnetization along the z direction. The magnetic textures correspond to the minimum of magnetic excitation energy at the zone-center (Γ point).

of the pitches are explained. In Figs. 4(a)–4(c), the ground-state commensurate and incommensurate spin-spiral textures are displayed after dynamically solving the full Hamiltonian. Here, the adjacent noncollinear atomistic spins are oriented at an angle of 120° with respect to each other, and thus, the magnetic ground state constitutes a three-dimensional (3D) 120° spin configuration. In Fig. S3 in the SM [39], the 3D 120° spin configurations are illustrated. To demonstrate the importance of the complete Hamiltonian in achieving the ground state, we have presented the spin-spiral textures by solving the spin Hamiltonian with several combinations, viz., only J [Figs. 4(d)–4(f)], $J + K$ [Figs. 4(g)–4(i)], and $J + \Gamma$ [Figs. 4(j)–4(l)]. The corresponding dynamical structure factors $S(q, \omega)$ with the detailed spin textures are plotted in Figs. S4–S9 in the SM [39].

A detailed observation of Fig. 4 evinces that, albeit the pitches and the overall types of the spin spirals remain the same for all three systems for all combinations, the 3D 120° spin configurations are stabilized only with the complete Hamiltonian. All these spin-dynamical ground states are simulated at an ultralow temperature of 0.001 K. With increasing temperature, we have investigated the evolution of the spin textures in Fig 5, where the temperature-induced increase of configurational entropy leads to a prominent presence of weathervane defects [39]. However, the spin-spiral textures remain intact up to 5 K, which is higher than the superconducting critical temperature T_c of this series.

Presence of such chiral magnetic states at finite temperatures may impart an important impact toward the analysis of the experimental observation of electronic magnetochiral anisotropic effects in CVS, where there is a sudden onset of unusually large chiral transport with lowering of temperature <35 K [5]. For such a centrosymmetric system, the mirror symmetries are experimentally observed to be inherently broken by the itinerant carriers in the correlated phases. Although, for CVS, the presence of time-reversal symmetry breaking is under scrutiny after the absence of any polar Kerr signal, as observed by Saykin *et al.* [4], the presence of other spontaneously broken symmetries cannot be ruled out. Occurrence of chiral magnetism and spin-spiral ground states in this series can be a potential reason behind the experimentally observed broken symmetries. It should also be noted that the structural instability and the respective distortion is quite weak, and there are disputes and debates accompanied with the yet undetermined low-temperature crystal structure [40–43]. Thus, the presence of such an inherent chiral dynamical magnetic structure in the kagome system may provide an answer to the simultaneous and spontaneous occurrence of time-reversal, mirror, and C_6 rotational symmetry breaking in the CO and SC phases.

In conclusion, for the first part of this comprehensive study of the V-based kagome stibnites [10], we addressed the effects of the formation of the local moments at the V sites in the kagome series AV_3Sb_5 (A = Cs, Rb, K) on their CO and

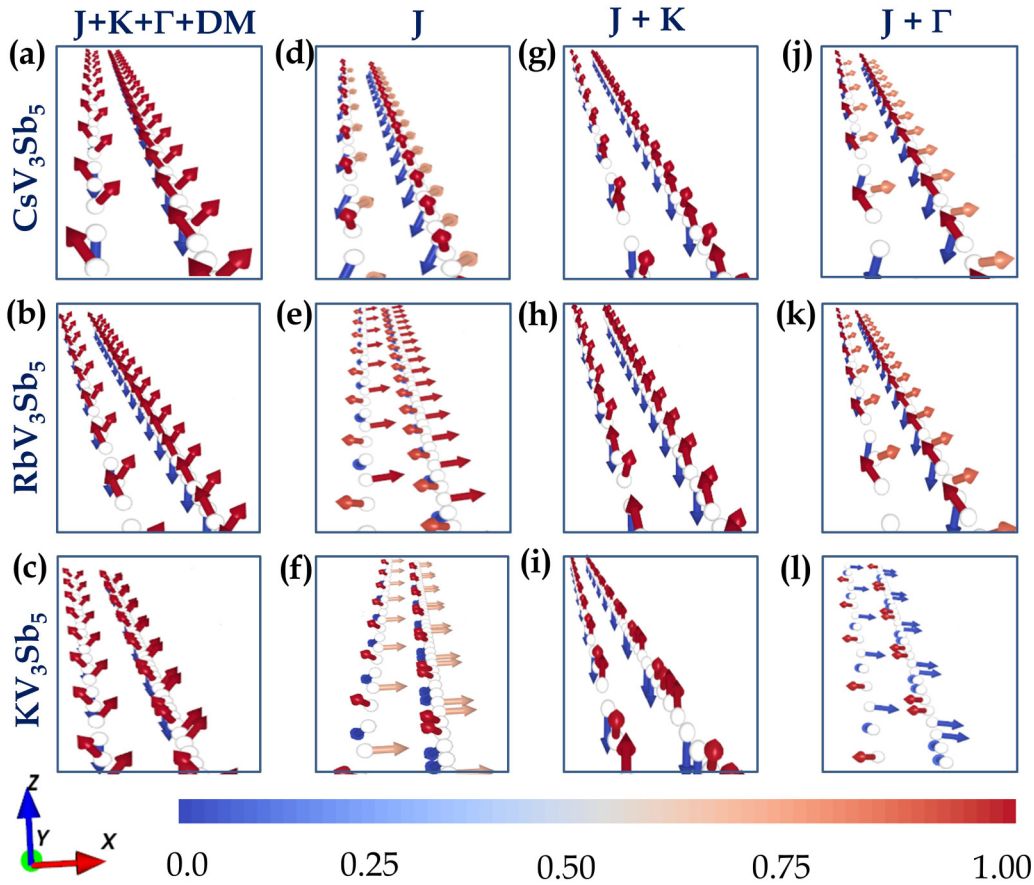

FIG. 4. (a)–(c) The three-dimensional (3D) view of the commensurate and incommensurate spirals with $J + K + \Gamma +$ DM Hamiltonian, (d)–(f) spin spirals with Hamiltonian having only J, (g)–(i) with $J + K$, and (j)–(l) with $J + \Gamma$ for CVS, RVS, and KVS respectively. For KVS, all the spirals are commensurate. The color bar indicates the projection of the magnetization along the z direction.

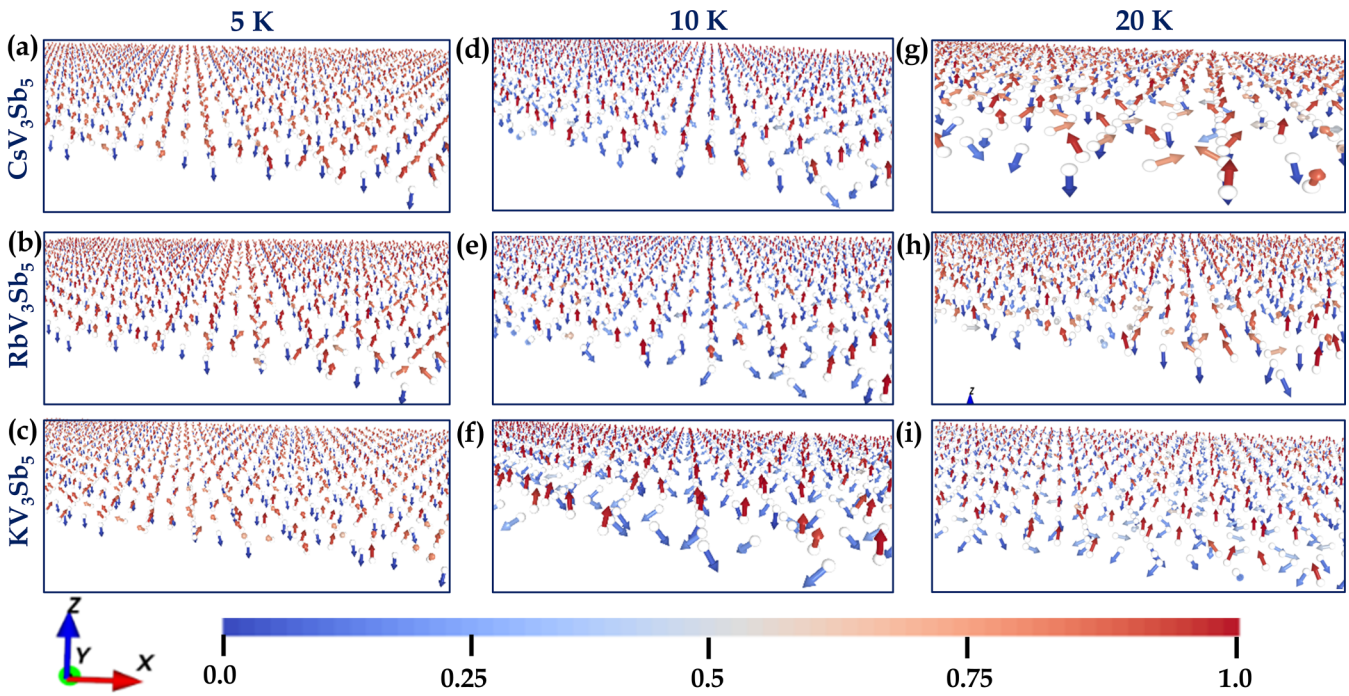

FIG. 5. The three-dimensional (3D) view of the magnetic ground-state spin textures at (a)–(c) 5 K, (d)–(f) 10 K, and (g)–(i) 20 K, for CVS, RVS, and KVS, respectively. All calculations include Heisenberg exchange and symmetric and antisymmetric anisotropic exchange interactions as well as magnetocrystalline anisotropy.

superconductivity [10]. In this second part, we have investigated the dynamical magnetic ground state of the system. The underlying arrangement of the spin-magnetic moments reveals that, in addition to the FM LRO along the [001] direction, there are complex landscapes of spin-spiral configurations in the [010] direction, consisting of commensurate and incommensurate chiral magnetic textures. The presence of such chiral magnetic textures has the capability of spontaneously breaking the time-reversal, mirror, or C_6 rotational symmetry and thus may provide a valid explanation to the experimental findings. In addition, the theoretically derived dynamical structure factors support the presence of complex, collective magnetic excitations within the system, which may be validated by future experimental studies. Thus, our thorough analysis of the dynamical aspects of the magnetism for the V-based kagome stibnites can be helpful in providing an explanation to the existing experimental queries and may also provide a motivation for future experimental studies.

Financial support from Vetenskapsrådet (Grants No. VR 2016-05980 and No. VR 2019-05304) and the Knut and Alice Wallenberg Foundation (Grants No. 2018.0060, No. 2021.0246, No. 2022.0108, and No. 2022.0079) is acknowledged. The computations were enabled by resources provided by the National Academic Infrastructure for Supercomputing in Sweden and the Swedish National Infrastructure for Computing at the National Supercomputer Centre and the PDC Center, partially funded by the Swedish Research Council through Grant Agreements No. 2022-06725 and No. 2018-05973. OE also acknowledges support from STandUPP and eSSENCE. DK acknowledges Bhabha Atomic Research Centre supercomputing facility. MNH acknowledges Council of Scientific and Industrial Research (India) for fellowship. IDM acknowledges support from the Junior Research Group Program at the Asia Pacific Center for Theoretical Physics through the Science and Technology Promotion Fund and Lottery Fund of the Korean Government as well as from the Korean Local Governments-Gyeongsangbuk-do Province and Pohang City. IDM and SS also acknowledge financial support from the National Research Foundation of Korea, funded by the Ministry of Science and ICT, through the Mid-Career Grant No. 2020R1A2C101217411.

[1] C. Mielke, D. Das, J. X. Yin, H. Liu, R. Gupta, Y. X. Jiang, M. Medarde, X. Wu, H. C. Lei, J. Chang *et al.*, Nature (London) **602**, 245 (2022).
[2] Y.-X. Jiang, J.-X. Yin, M. M. Denner, N. Shumiya, B. R. Ortiz, G. Xu, Z. Guguchia, J. He, M. S. Hossain, X. Liu *et al.*, Nat. Mater. **20**, 1353 (2021).
[3] S.-Y. Yang, Y. Wang, B. R. Ortiz, D. Liu, J. Gayles, E. Derunova, R. Gonzalez-Hernandez, L. Šmejkal, Y. Chen, S. S. P. Parkin *et al.*, Sci. Adv. **6**, eabb6003 (2020).
[4] D. R. Saykin, C. Farhang, E. D. Kountz, D. Chen, B. R. Ortiz, C. Shekhar, C. Felser, S. D. Wilson, R. Thomale, J. Xia *et al.*, Phys. Rev. Lett. **131**, 016901 (2023).
[5] C. Guo, C. Putzke, S. Konyzheva, X. Huang, M. Gutierrez-Amigo, I. Errea, D. Chen, M. G. Vergniory, C. Felser, M. H. Fischer *et al.*, Nature (London) **611**, 461 (2022).
[6] W. Schweika, M. Valldor, and P. Lemmens, Phys. Rev. Lett. **98**, 067201 (2007).
[7] D. Boyko, A. Saxena, and J. T Haraldsen, Ann. Phys. (Berlin) **532**, 1900350 (2019).
[8] M. Taillefumier, J. Robert, C. L. Henley, R. Moessner, and B. Canals, Phys. Rev. B **90**, 064419 (2014).
[9] M. Nishiyama, S. Maegawa, T. Inami, and Y. Oka, Phys. Rev. B **67**, 224435 (2003).
[10] J. Becker and S. Wessel, Phys. Rev. B **100**, 241113(R) (2019).
[11] T. Xie, Q. Yin, Q. Wang, A. I. Kolesnikov, G. E. Granroth, D. L. Abernathy, D. Gong, Z. Yin, H. Lei, and A. Podlesnyak, Phys. Rev. B **106**, 214436 (2022).
[12] M. N. Hasan, R. Bharati, J. Hellsvik, A. Delin, S. K. Pal, A. Bergman, S. Sharma, I. Di Marco, M. Pereiro, P. Thunström, P. M. Oppeneer, O. Eriksson, and D. Karmakar, companion paper, Phys. Rev. Lett. **131**, 196702 (2023).
[13] M. Ležaić, P. Mavropoulos, G. Bihlmayer, and S. Blügel, Phys. Rev. B **88**, 134403 (2013).
[14] A. I. Liechtenstein, M. I. Katsnelson, V. P. Antropov, and V. A. Gubanov, J. Magn. Magn. Mater. **67**, 65 (1987).
[15] Y. O. Kvashnin, O. Grånäs, I. Di Marco, M. I. Katsnelson, A. I. Lichtenstein, and O. Eriksson, Phys. Rev. B **91**, 125133 (2015).
[16] Y. O. Kvashnin, A. Bergman, A. I. Lichtenstein, and M. I. Katsnelson, Phys. Rev. B **102**, 115162 (2020).
[17] A. Grechnev, I. Di Marco, M. I. Katsnelson, A. I. Lichtenstein, J. Wills, and O. Eriksson, Phys. Rev. B **76**, 035107 (2007).
[18] P. Thunström, I. Di Marco, and O. Eriksson, Phys. Rev. Lett. **109**, 186401 (2012).
[19] J. M. Wills, M. Alouani, P. Andersson, A. Delin, O. Eriksson, and O. Grechnyev, *Full-Potential Electronic Structure Method: Energy and Force Calculations with Density Functional and Dynamical Mean Field Theory* (Springer-Verlag, Berlin, 2010), Vol. 167.
[20] A. Szilva, Y. Kvashnin, E. A. Stepanov, L. Nordström, O. Eriksson, A. I. Lichtenstein, and M. I. Katsnelson, Rev. Mod. Phys. **95**, 035004 (2023).
[21] M. Udagawa and Y. Motome, Phys. Rev. Lett. **104**, 106409 (2010).
[22] L. Messio, B. Bernu, and C. Lhuillier, Phys. Rev. Lett. **108**, 207204 (2012).
[23] M. Bode, M. Heide, K. von Bergmann, P. Ferriani, S. Heinze, G. Bihlmayer, A. Kubetzka, O. Pietzsch, S. Blügel, and R. Wiesendanger, Nature (London) **447**, 190 (2007).
[24] B. Zimmermann, M. Heide, G. Bihlmayer, and S. Blügel, Phys. Rev. B **90**, 115427 (2014).
[25] S. Heinze, K. von Bergmann, M. Menzel, J. Brede, A. Kubetzka, R. Wiesendanger, G. Bihlmayer, and S. Blügel, Nat. Phys. **7**, 713 (2011).
[26] N. Romming, C. Hanneken, M. Menzel, J. E. Bickel, B. Wolter, K. von Bergmann, A. Kubetzka, and R. Wiesendanger, Science **341**, 636 (2013).
[27] A. Neubauer, C. Pfleiderer, B. Binz, A. Rosch, R. Ritz, P. G. Niklowitz, and P. Böni, Phys. Rev. Lett. **102**, 186602 (2009).

[28] C. Franz, F. Freimuth, A. Bauer, R. Ritz, C. Schnarr, C. Duvinage, T. Adams, S. Blügel, A. Rosch, Y. Mokrousov *et al.*, Phys. Rev. Lett. **112**, 186601 (2014).
[29] T. Schulz, R. Ritz, A. Bauer, M. Halder, M. Wagner, C. Franz, C. Pfleiderer, K. Everschor, M. Garst, and A. Rosch, Nat. Phys. **8**, 301 (2012).
[30] S. Emori, U. Bauer, S.-M. Ahn, E. Martinez, and G. S. D. Beach, Nat. Mater. **12**, 611 (2013).
[31] R. M. Otxoa, P. E. Roy, R. Rama-Eiroa, J. Godinho, K. Y. Guslienko, and J. Wunderlich, Commun Phys **3**, 190 (2020).
[32] K.-S. Ryu, L. Thomas, S.-H. Yang, and S. Parkin, Nat. Nanotech. **8**, 527 (2013).
[33] C. Etz, L. Bergqvist, A. Bergman, A. Taroni, and O. Eriksson, J. Phys.: Condens. Matter **27**, 243202 (2015).
[34] B. Skubic, J. Hellsvik, L. Nordström, and O. Eriksson, J. Phys.: Condens. Matter **20**, 315203 (2008).
[35] P. Kurz, F. Förster, L. Nordström, G. Bihlmayer, and S. Blügel, Phys. Rev. B **69**, 024415 (2004).
[36] J. C. Leiner, T. Kim, K. Park, J. Oh, T. G. Perring, H. C. Walker, X. Xu, Y. Wang, S. W. Cheong, and J.-G. Park, Phys. Rev. B **98**, 134412 (2018).
[37] S. Petit, JDN **12**, 105 (2011).
[38] S. Toth and B. Lake, J. Phys.: Condens. Matter **27**, 166002 (2015).
[39] See Supplemental Material at http://link.aps.org/supplemental/10.1103/PhysRevB.108.174413 for the description of the commensurate and incommensurate spirals, the 120° structures, the spin-textures with different terms of the full spin Hamiltonian, and the corresponding dynamical structure factor plots.
[40] H. Zhao, H. Li, B. R. Ortiz, S. M. L. Teicher, T. Park, M. Ye, Z. Wang, L. Balents, S. D. Wilson, and I. Zeljkovic, Nat. (London) **599**, 216 (2021).
[41] B. R. Ortiz, S. M. L. Teicher, Y. Hu, J. L. Zuo, P. M. Sarte, E. C. Schueller, A. M. M. Abeykoon, M. J. Krogstad, S. Rosenkranz, R. Osborn *et al.*, Phys. Rev. Lett. **125**, 247002 (2020).
[42] J. Luo, Z. Zhao, Y. Z. Zhou, J. Yang, A. F. Fang, H. T. Yang, H. J. Gao, R. Zhou, and G-Q Zheng, npj Quantum Mater. **7**, 30 (2022).
[43] Q. Stahl, D. Chen, T. Ritschel, C. Shekhar, E. Sadrollahi, M. C. Rahn, O. Ivashko, M. v. Zimmermann, C. Felser, and J. Geck, Phys. Rev. B **105**, 195136 (2022).